

18 JUN 1982

①

GREGORY & PEARSON

AD A117482

ANALYTICAL AND EXPERIMENTAL STUDIES OF THE RESPONSE
OF A CYLINDER TO NUCLEAR THERMAL/BLAST LOADS (U)

*FREDERICK H. GREGORY, MR.
RICHARD J. PEARSON, MR.
U.S. ARMY BALLISTIC RESEARCH LABORATORY
ABERDEEN PROVING GROUND, MARYLAND 21005

Two phenomena which are emitted from a nuclear weapon, whose target vulnerability ranges often overlap, are thermal radiation and blast waves. In most situations of interest to the Army, targets are exposed to a high percentage of the total available thermal pulse prior to blast wave arrival. This sequence of loads is detrimental to the survival of light weight structures in which significant in-depth heating occurs prior to the blast wave envelopment. There has been evidence that this thermal preheating causes enhanced structural damage [1,2].

EXPERIMENT DESCRIPTION

In order to demonstrate these types of synergistic responses and to provide some quantitative data, three experiments have been conducted on hollow cylinders of aluminum 6061-T6 in the BRL Thermal/Blast Simulator. One experiment was conducted with thermal-only exposure, one with blast-only loading, and one with combined thermal/blast loading. A diagram of the Simulator is shown in Figure 1. The target cylinder is clamped at each end and placed with its axis in a vertical position as shown. The thermal source is situated downstream from the target to minimize the effects of the shock passing through heated air and combustion products. In the combined thermal/blast test, the target is rotated through 180° so that the heated side of the target cylinder is exposed to the on-coming shock wave.

The thermal heating of the aluminum cylinder is accomplished by burning of a mixture of aluminum powder and oxygen. Two thin plastic membranes serve to contain the oxygen gas before ignition. The aluminum powder is sprayed through nozzles into the oxygen atmosphere and ignited starting with the nozzles farthest from the target. The aluminum oxide particles resulting from the burn irradiated the near side of the cylinder, raising its temperature by approximately 200°C.

The shock loading on the cylinder is produced by pressurizing the driver section of the shock tube shown in Figure 1 and then explosively

DTC FILE COPY

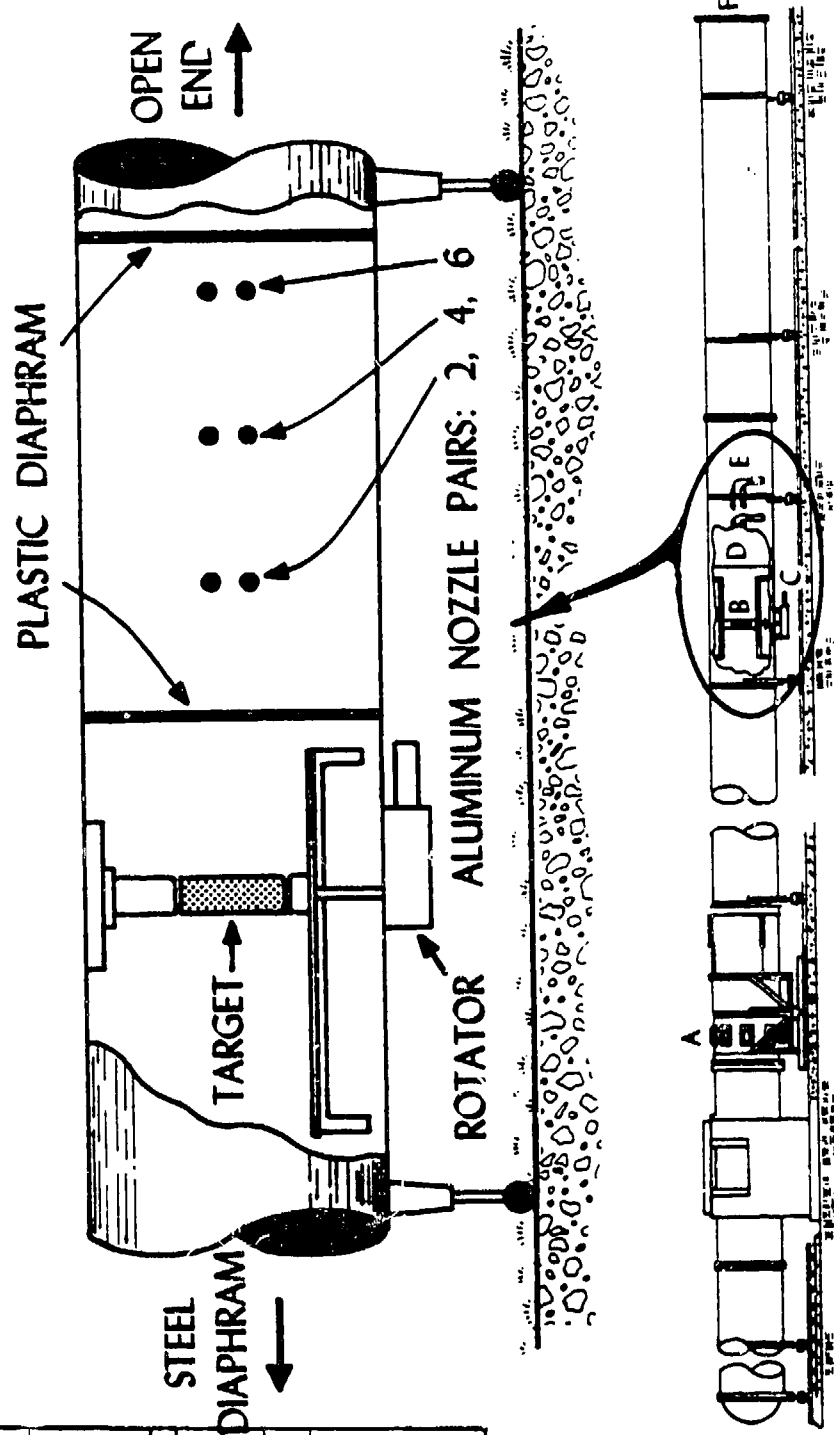
DTIC
ELECTE
JUL 26 1982

This document has been approved
for public release and sale; its
distribution is unlimited.

82 07 19 268

Accession For	<input checked="" type="checkbox"/>
NTIS GRA&I	<input type="checkbox"/>
DTIC TAB	<input type="checkbox"/>
Unannounced	<input type="checkbox"/>
Justification	
By	
Distribution/	
Availability Codes	
Avail and/or	
Special	
1st	A

DTIC
COPY
INSPECTED
&



A. STEEL DIAPHRAM . B. TARGET D. PLASTIC DIAPHRAM F. OPEN END OF TUBE
C. ROTATOR E. FLUIDIZERS

Figure 1. Ballistic Research Laboratory Thermal/Blast Simulator Facility

RE: Classified References, Distribution Unlimited
No change in distribution statement per Ms. Ann Taylor, ARO

perforating the steel diaphragm at the interface of the driver section and the expansion section (Item A in Figure 1). Despite the fact that the thermal source was located downstream from the target, some degradation of the leading spike of the shock wave occurred due to the presence of heated air in the vicinity of the cylinder.

The following measurements were made on the cylinder during the tests: pressure, axial and circumferential strain, temperature, and thermal flux. In addition, two high speed cameras were used to monitor the sequence of events occurring in the simulator. Pre- and post-shot measurements of the radius of the cylinders were made at 384 points on each cylinder. More detailed descriptions of the instrumentation are contained in Reference 3.

The cylindrical targets were made from 1.016 mm thick sheets of aluminum 6061-T6. The sheets were formed into cylinders and seam welded on the side farthest from the loading side. The inside diameter of the cylinders was 30.48 cm (12 inches) and the length between upper and lower clamps was 80 cm. In order to make the ADINA finite element modeling of the experiments easier, the upper and lower ends of the cylinders were clamped securely in heavy steel end discs. The end discs were connected by shafts to bearings. The bearings were mounted in two heavy bearing mounts. To minimize the disturbance of the flow past the cylinder, the mounts were made with the same outer diameter as the target cylinders.

NUMERICAL MODEL

The numerical modeling of these tests was done with the ADINA finite element program [4]. The element type used was the 3-D brick element, which has a thermo-elastic formulation. Symmetry was assumed about a plane passing through the cylinder axis oriented in the direction of air-heat flow. Another plane of symmetry was assumed passing orthogonal to both the previous plane and passing through the Z-coordinate $L/2$, where L is the active length of the cylinder. With these assumptions, only one quarter of the cylinder was required for the finite element model. Actually, there was approximately a 10 per cent variation in heating along the axis of the cylinder due to nearby reflecting surfaces. However, this variation was ignored in the numerical simulation.

The quarter cylinder was modeled with 72 brick elements, 8 in the axial direction, 9 in the circumferential direction, and 1 in the thickness direction. The elements had a midside node on each edge and the number of integration points in the element was 3 in each direction, for a total of 27 per element. The outside surface of the undeformed mesh is indicated in Figure 2 by the crosses and dotted lines. The crosses represent the nodal points on the outside surface and the dotted lines are the undeformed mesh boundaries.

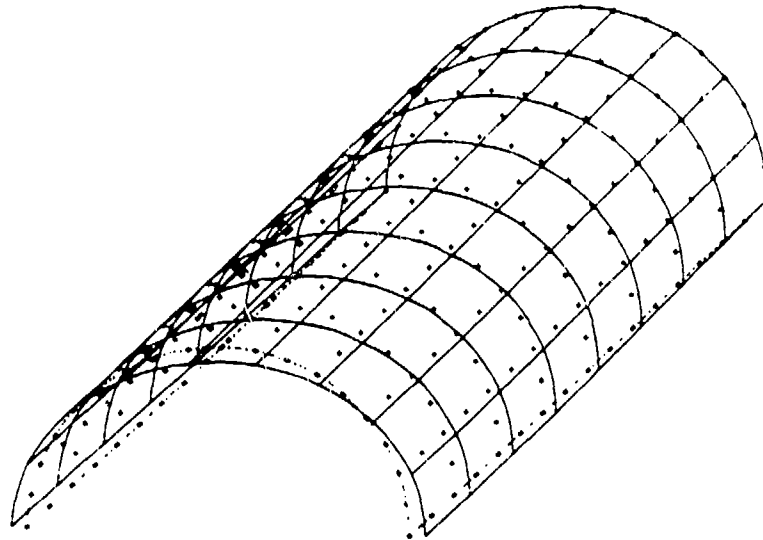


Figure 2. Mode Shape for the 7th Eigenfrequency (3961 cycles/seconds)

The lower eigenfrequencies and mode shapes were evaluated for use in a mode superposition analysis of the elastic response of the cold cylinder. Knowing the periods of the lower eigenfrequencies is also useful in determining the approximate time required for a peak deflection to occur. The periods determined ranged from 3.66 ms for the lowest mode to 1.47 ms for the eleventh mode. Shown in Figure 2 is mode number seven, which has the simplest geometric shape (egg-shaped cross section).

The finite element calculations for the dynamic response of the cylinder were made using the explicit central difference time marching scheme. The time step was obtained from the Courant stability condition,

$$\Delta t = \frac{\Delta l}{\sqrt{E_y/\rho}}$$

where Δl is the distance between the two closest nodes, E_y is Young's modulus, and ρ is the material density. For the higher order elements used here, we found that this time increment was unstable and we used one half of the Courant Δt , which was stable. This time increment was 50 ns.

The constitutive properties of the cold aluminum 6061-T6 material were measured in an Instron testing machine. Tensile test specimens were cut from the same sheet of material used for fabrication of the cylinders. Properties were measured in the rolling direction and perpendicular to the

GREGORY & PEARSON

rolling direction. The average of these tensile properties was used in the ADINA calculations. Properties measured in this way were the Young's modulus, bilinear corner yield stress, plastic modulus and Poisson's ratio.

Dynamic temperature dependent constitutive properties were measured in the DNA Tri-Service Flash Test Facility. In these tests, samples of the material were heated in a fraction of a second and strained through the yield point several seconds later. These times were close to the temperature-time sequence experienced in the thermal/blast simulation tests. The yield points determined in these tests were consistent with other data [5]. However, the plastic tangent moduli appeared to be higher than expected. Due to this result and to difficulty in keeping strain gages bonded at the high temperatures, we chose to await further confirmation prior to using the data. The following temperature dependent stress-strain data have been derived from Reference 5. No temperature dependent data for

Temperature °C	Density g/cm ³	Yield MPa	Young's Modulus GPa
28	2.703	301.0	64.73
100	2.689	275.4	62.20
150	2.678	259.1	60.80
200	2.667	240.5	59.29

the plastic tangent modulus and Poisson's ratio were available. The cold properties measured in the Instron testing machine of 650 MPa and 0.3285, respectively, were used for all temperature ranges.

The ADINA calculations were performed using a bilinear von Mises kinematic hardening material model. This model required the specification of the materials properties: Young's modulus, Poisson's ratio, initial yield stress, and plastic tangent modulus.

RESULTS

The three types of tests and analyses will be discussed in the same order as the experiments were performed. The input head-on pressure for the blast-only test is shown in Figure 3. The maximum stagnation overpressure was 60 kPa. Shown in Figure 4 is the short term reflected pressure on the cylinder at zero degrees. The peak load is 104 kPa (15 psi). Figure 5 shows the pressure loading on the side of the cylinder (90°). Loading data were recorded at 15° intervals around the cylinder. Since the finite element calculations required loading at 20° intervals around the circumference starting at 10°, these data were interpolated in both circumferential angle and time to supply the pressure loading for ADINA.

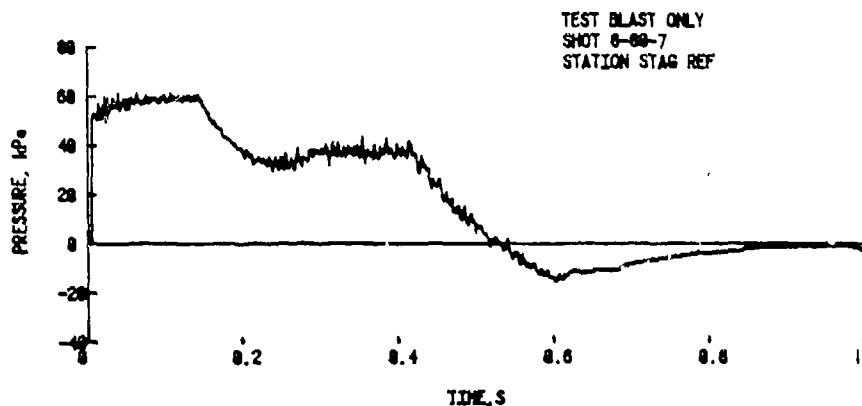


Figure 3. Blast-Only Test, Head-On Pressure

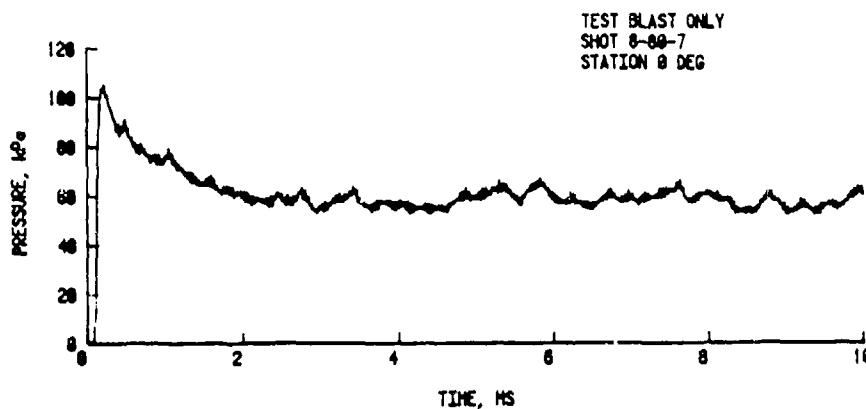


Figure 4. Blast-Only Test, Diffraction Phase Loading at 0°

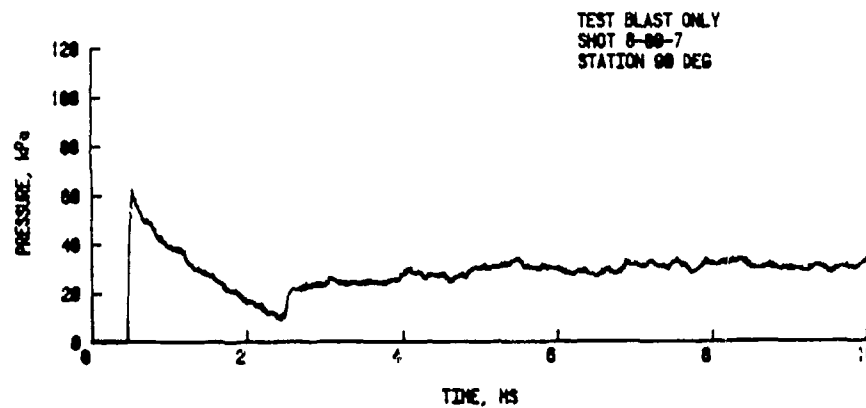


Figure 5. Blast-Only Test, Diffraction Phase Loading at 90°

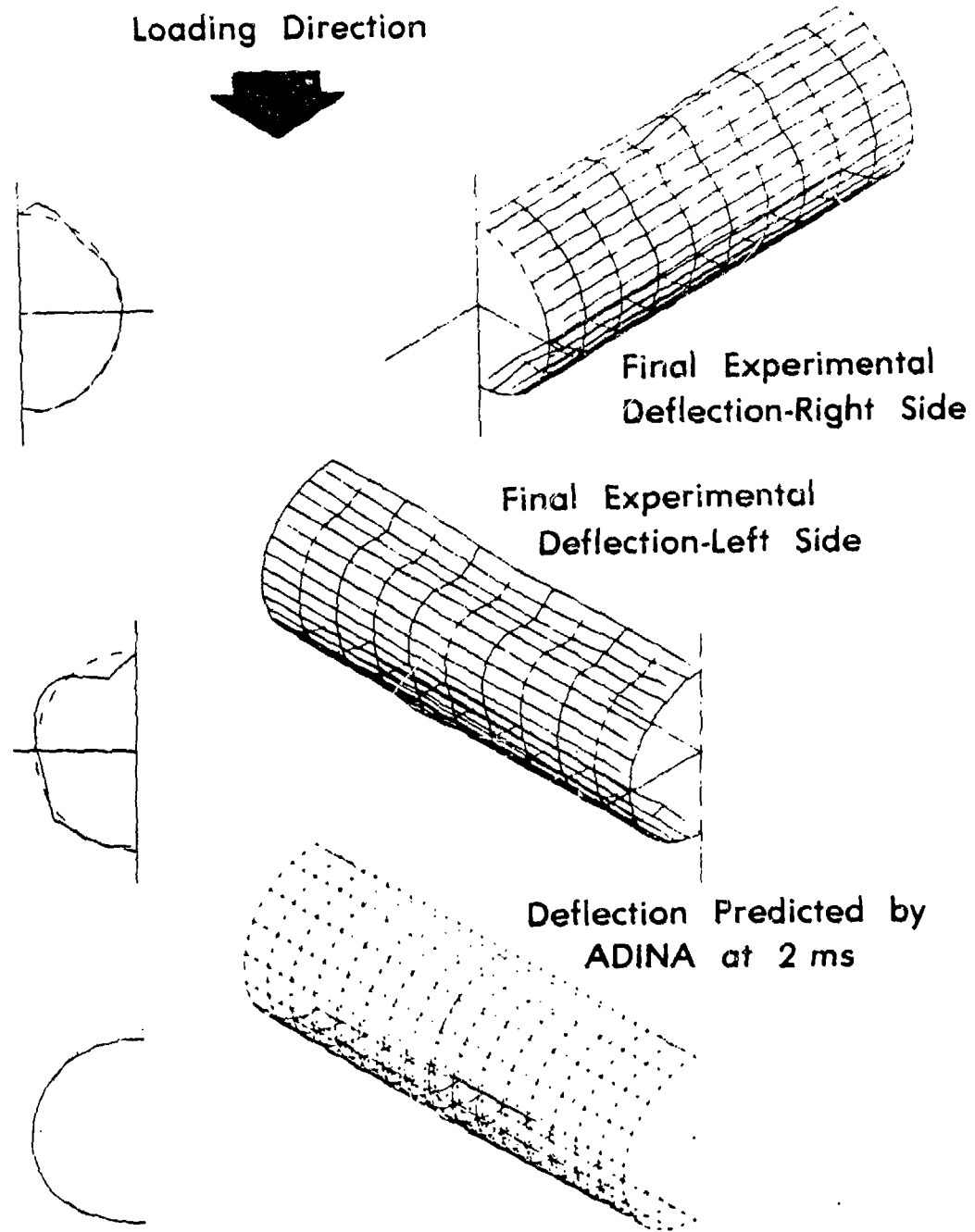
Experimental measurements of the final radial deflection of the cylinder to the blast load were made and the results are shown in the top and middle part of Figure 6 for the right and left halves of the cylinder. The deflections shown have been magnified by a factor of ten to make the deformed shape more apparent. Deformation of the actual cylinder was barely noticeable to the eye. The resulting deformation pattern was only approximately symmetric about the zero degree line and about a plane at $Z = L/2$. For Figure 6, the loading direction is from the top for all three parts of the figure. The deformed shapes for the three subplots at the $Z = L/2$ center cross section are shown on the left side of Figure 6. The ADINA calculations have been carried out to 2.0 ms and the deflection pattern at that time is shown on the right side of Figure 6. Since no plasticity was observed in this calculation, this is not the final predicted shape of the cylinder, but is approximately the maximum deflection occurring during the excitation of the simulated cylinder.

In the second test, the cylinder was exposed to a thermal load only. Shown in Figure 7 is the flux and the fluence received by the flux gage positioned off to the side of the cylinder. The solid line is the flux as recorded by the gage. The fluence was obtained by integrating the flux curve. The nominal 25 cal/cm² fluence on the target was obtained by relating the fluence to previous calibration tests. Figures 8 and 9 show the temperature rise indicated by thermocouples at $Z = L/2$, $\theta = 0^\circ$ and 90° respectively. The nominal temperature rise was 225°C at 0° and 45°C at 90° .

The ADINA model for the thermal-only loading was the same mesh configuration as for the blast-only loading. However, instead of the pressure load applied to the exterior of the cylinder, an initial displacement of the Z-coordinates of the cylinder proportional to the temperature increase was assumed. A prescribed displacement was applied to the symmetry end of the cylinder at $Z = L/2$. This artifice was used in lieu of performing an ADINAT [6] calculation to determine the temperature in the cylinder as a function of time. Earlier calculations using ADINAT showed that the heat penetrates through the thickness of 1.016 mm in a time which is short compared to the structural response time. Based on this result, temperature was assumed to reach equilibrium through the thickness instantaneously. Initial displacements were calculated for each nodal point based on the fluence received at that point. The displacements were calculated relative to the fixed end according to the formula

$$w(\theta, Z) = \frac{Z\alpha}{h\rho C} \int_0^{\infty} \phi(\theta, t) dt,$$

where α is the coefficient of thermal expansion, h is the thickness, ρ is the density, C is the heat capacity, and $\phi(\theta, t)$ is the incident flux.



Deflection Magnification 10X

Figure 6. Comparison of Experimental and Predicted Deflections, Magnified 10X, Blast-Only Loading

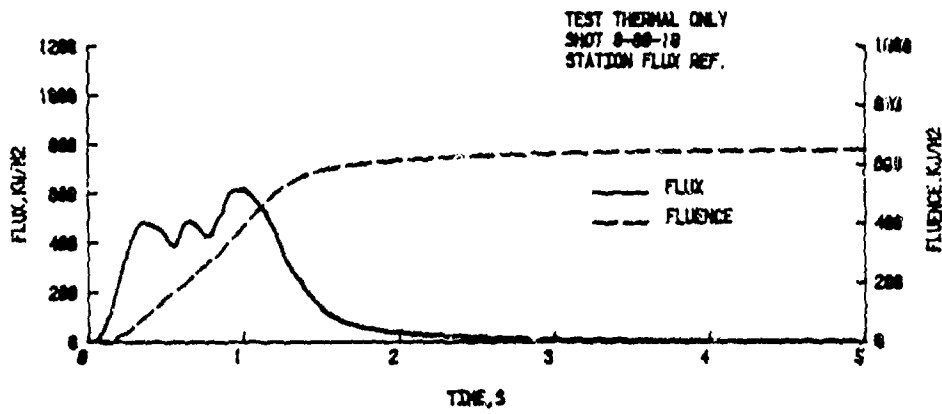


Figure 7. Reference Flux and Fluence

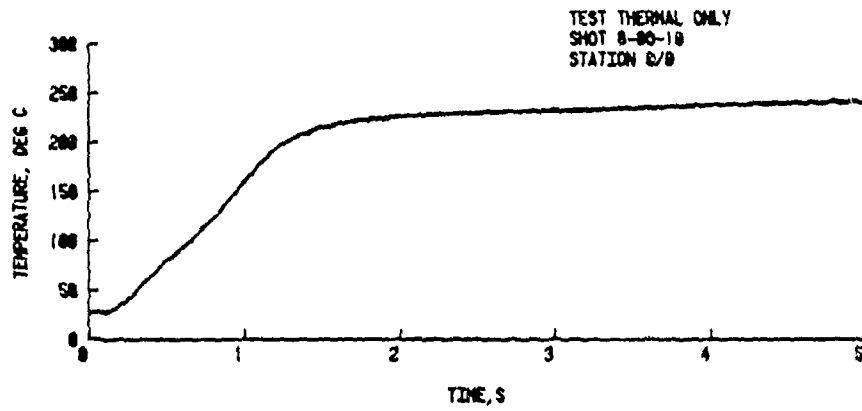


Figure 8. Temperature History at $Z = L/2$, $\theta = 0^\circ$

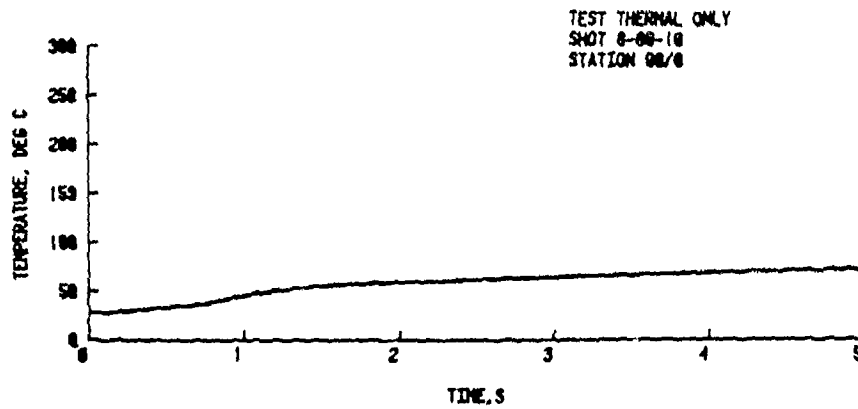


Figure 9. Temperature History at $Z = L/2$, $\theta = 90^\circ$ for Thermal-Only Loaded Cylinder

Measurements on the post-test thermally loaded cylinder showed a slight degree of buckling near the ends of the cylinder on the near side. The deformation pattern is shown in the top two subplots of Figure 10 and is nearly symmetric in both the Z and θ coordinates. The displacements from the original geometric positions are magnified by 10X in Figure 10. The deflection was small and was most apparent to the unaided eye near each end where the largest changes in slope occurred. The deformation cross sections at the mid-point, $Z = L/2$, are shown on the left side of Figure 10. The displacement was outward at $\theta = 0^\circ$ and inward at $\theta = 90^\circ$.

The ADINA simulation of the thermally loaded cylinder was carried out to 1.1 ms. Plasticity occurred early in the calculation and peak deflections were observed at approximately 0.725 ms. The deformed shape at this time as predicted by ADINA is shown in the lower part of Figure 10. The apparent cut shown in Figure 10 at $Z = L/2$ is the prescribed constant Z -displacement which simulates the thermal expansion. The prescribed displacement ranged from 1.8 mm at $\theta = 0^\circ$, zero at $\theta = 120^\circ$. The deformation cross section at $Z = L/2$ showed a similar trend as did the experimental results. However, no buckling was predicted by ADINA near the $Z = L/20$ point, contrary to what was observed in the experiment. An incipient buckling deflection of approximately twice the cylinder thickness appeared to be forming at $Z = L/2$, $\theta = 100^\circ$ in the ADINA results.

In the final test in the BRL Thermal/Blast Simulator, the cylinder was exposed to the thermal radiation, rotated and exposed to the air shock. The reference flux and temperature histories at 0° and 90° are shown in Figures 11-13. The long term stagnation pressure record is shown in Figure 14. The pressure loadings on the cylinder at $\theta = 0^\circ$ and 90° are shown in Figure 15 and 16. Comparing Figures 15 and 16 with Figures 4 and 5, one notices that the pressure load rises much more gradually in the presence of the heated air surrounding the cylinder. From Figures 14 and 3, one sees that the long term pressure produced by the shock tube is only slightly less for the thermal/blast test than was the case for the blast-only test. As shown in Figures 12 and 8, the peak temperature rise in thermal/blast test was 170°C and in the thermal-only test it was 225°C .

The final deformed shape of the cylinder after the combined thermal/blast test is shown in Figure 17. The deformation is symmetric with respect to the two symmetry planes. The deflection magnification in Figure 17 is only 5X, one half of the magnification used in Figures 6 and 10. At $Z = L/2$, the peak radial deflection for the thermal/blast test is approximately 4 times as large as for the blast-only deflection and 10 times as large as the thermal-only deflection. ADINA calculations for the thermal/blast simulation have not been made and no comparisons are available.

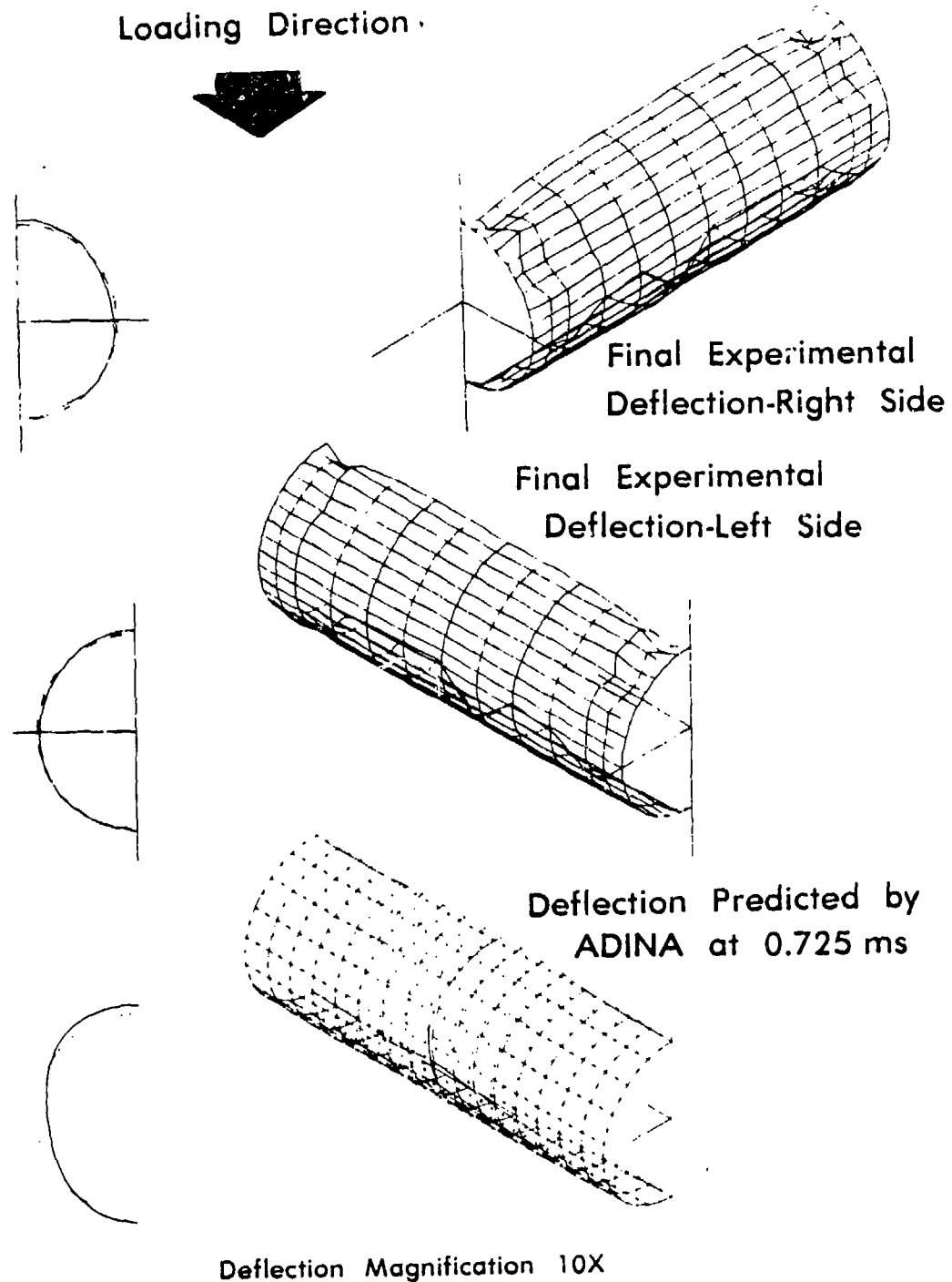


Figure 10. Comparison of Experimental and Predicted Deflections, Magnified 10X, Thermal-Only Loading

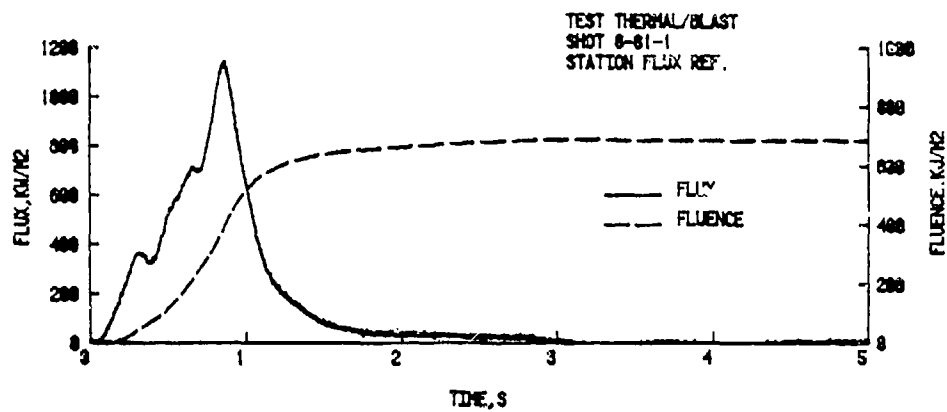


Figure 11. Thermal/Blast Test, Reference Flux and Fluence

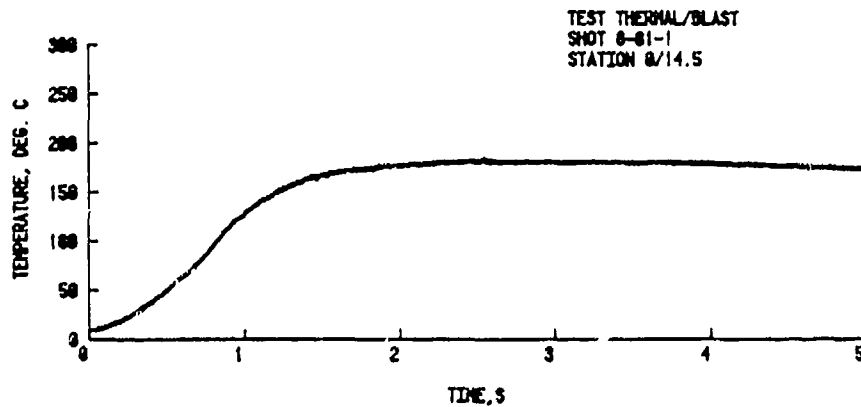


Figure 12. Thermal/Blast Test, Temperature History at $Z = L/10$, $\theta = 0^\circ$

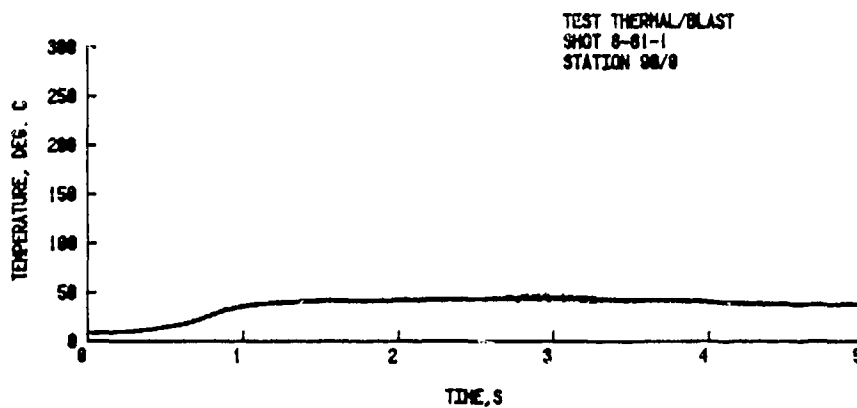


Figure 13. Thermal/Blast Test, Temperature History at $Z = L/2$, $\theta = 90^\circ$

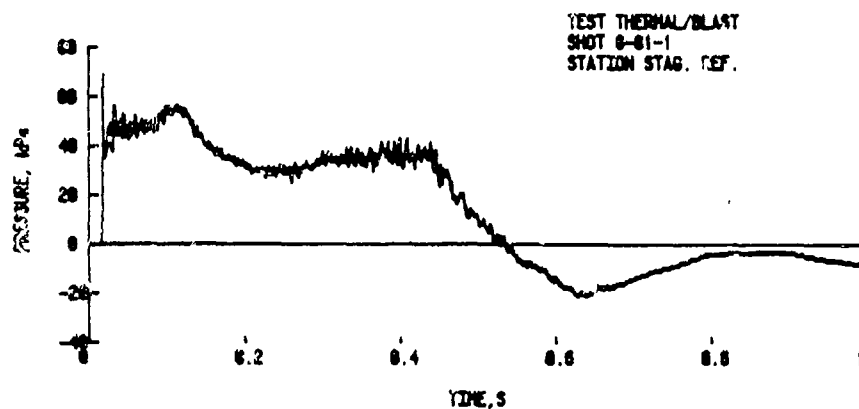


Figure 14. Thermal/Blast Test, Head-On Pressure

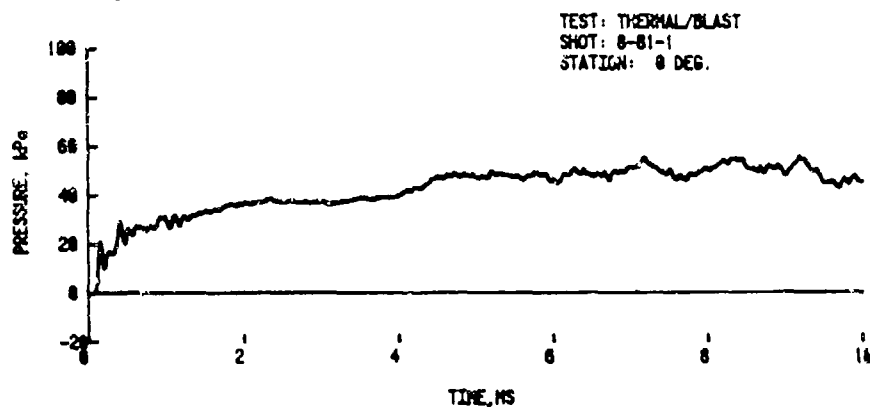


Figure 15. Thermal/Blast Test, Diffraction Phase Loading at 0°

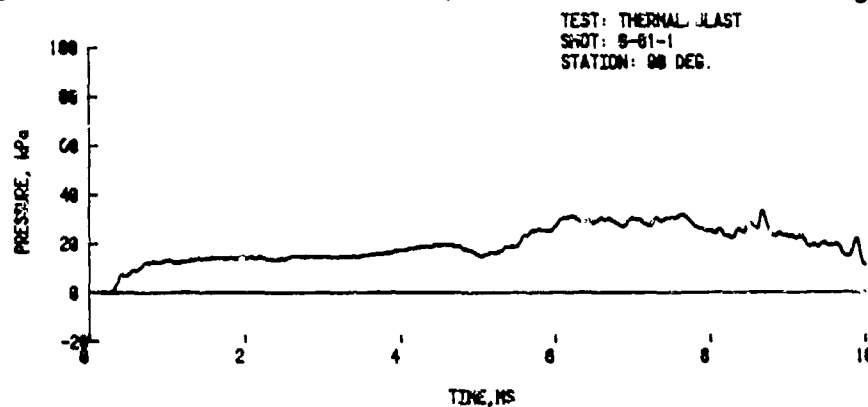
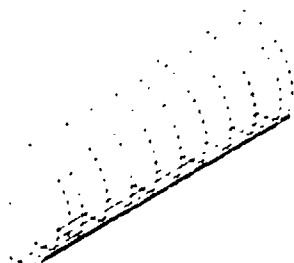


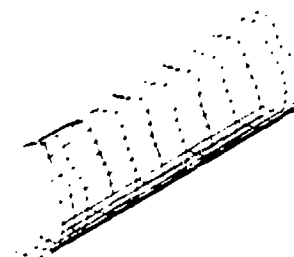
Figure 16. Thermal/Blast Test, Diffraction Phase Loading at 90°

GREGORY & PEARSON

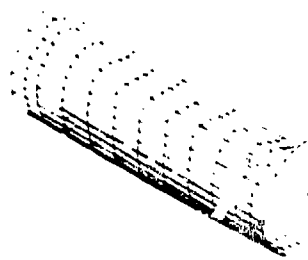
LOADING DIRECTION



PRE-TEST TARGET SHAPE - RIGHT HALF



POST-TEST TARGET SHAPE - RIGHT HALF



POST-TEST TARGET SHAPE - LEFT HALF

DEFLECTION MAGNIFICATION 5X

Figure 17. Comparison of Pre-Test and Post-Test Shapes for Thermal/Blast Test

CONCLUSIONS

The series of tests showed that the effect of combined thermal and blast loadings at realistic time separations produces a nonlinear response in thermally thin targets. Moreover, the shape of the deformed cylinders is markedly different between the three tests. The heated cylinder tended to displace outward on the near and far sides; whereas, the combined test resulted in a dished-in surface on the near side.

The results obtained thus far with ADINA are not as satisfying as was originally expected. However, the permanent deflections produced in both the thermal-only and blast-only tests were very small. Furthermore, the general shape of the deformations predicted by ADINA was correct. It is evident that we need to develop a Kirchhoff shell element whose stable time step is not limited by the rotatory inertia. This would improve the efficiency of the ADINA calculation significantly.

REFERENCES

1. P. J. Morris, "A Review of Research on Thermal Radiation Degradation of Structural Resistance to Air Blast," (U), URS Research Company, DNA-2856F, December 1971 (SECRET).
2. D. M. Wilson, "The Distribution and History of Temperature in Circular Cylinders Exposed to the Thermal Radiation Pulse of a Nuclear Detonation," NOLTR-71-61, June 1971.
3. R. J. Pearson, et al. "Synergism in Nuclear Thermal/Blast Loading," Seventh International Symposium on Military Applications of Blast Simulation, Medicine Hat, Alberta, Canada, July 1981.
4. K. J. Bathe, "ADINA, A Finite Element Program for Automatic Dynamic Incremental Analysis," MIT-82448-1, December 1978.
5. T. Stefansky, et al. "Temperature Induced Degradation of Mechanical Properties Following Instantaneous Heating," AFWL-TR-71-62, Sep 1977.
6. K. J. Bathe, "ADINAT, A Finite Element Program for the Automatic Dynamic Incremental Nonlinear Analysis of Temperatures," MIT-82448-5, Dec. 1978.